Research Article

Feng Wu*, Cong Yao, Linlin Cong, and Yanping Xi

Pore-scale gas–water flow in rock: Visualization experiment and simulation

https://doi.org/10.1515/geo-2020-0105
received August 16, 2019; accepted March 23, 2020

Abstract: The characteristics of pore-scale two-phase flow are of significance to the effective development of oil and gas resources, and visualization has gradually become one of the hot spots in the research of pore-scale two-phase flow. Based on the pore structure of rock, this research proposed a microscopic glass etching displacement experiment and a Navier–Stokes equation based finite element simulation to study the pore-scale gas–water two-phase flow. Then, this research conducted the proposed methods on the type I, type II and type III tight sandstone reservoirs in the Penglaizhen Formation of western Sichuan Basin, China. Results show that the outcomes of both the microscopic glass etching displacement experiment and the finite element simulation are by and large consistent. The water distributed in the large pores is displaced, and the trapped water mainly exists in the area induced by flow around high-permeability pores, perpendicular pores and disconnected ends of pores. The microscopic glass etching displacement experiment is conducive to better observing the phenomenon of a viscous finger-like breakthrough and air jumps in migration flows in narrow throats, while the finite element simulation has the advantages of cost effectiveness, easy operation and strong experimental reproducibility.

Keywords: pore structure, gas–water two-phase flow, glass etching displacement model, finite element stimulation, Navier–Stokes equations, tight sandstone, Sichuan Basin

1 Introduction

The pore-scale two-phase flow in porous media plays a vital role in the fields of oil–gas resource development, tunneling, levee seepage prevention, chemical engineering [1–5], etc. Regarding oil and gas resource development, the pore-scale two-phase flow has a great impact on the studies of seepage mechanisms and recovery ratio improvement [1,6–8]. In recent years, researchers have conducted a great deal of research on pore-scale two-phase flow in rock, among which visualization has gradually become one of the hot spots [9,10]. In this context, there are two major research methods: physical observation experiment [11–15] and numerical simulation [16–19].

Currently, physical observation experiments on pore-scale two-phase flow are mainly based on the two-dimensional pore structure characteristics, including the core plug displacement based CT scan experiment [20,21], slabbed core sample based microscopic displacement experiment [11] and microscopic glass etching displacement experiment [12,13]. By applying the CT scanning technique, the core plug displacement based CT scan experiment can observe the fluid displacement process in the core plug indirectly. This method can obtain information concerning the fluid distribution and the advantageous displacement channel. Nevertheless, the resolution of the CT scan is usually too low to clearly display the pore-scale displacement and flow characteristics, which makes it hard to satisfy the needs for detailed studies of oil–gas development. In recent years, with the improvement of the resolution of the CT scan, scientists can visualize the fluid flow with a spatial resolution of 1 μm and a time resolution of 1 s. However, the spatial resolution is still not enough to describe the rocks with smaller size throats, such as tight

* **Corresponding author: Feng Wu,** School of Geoscience and Technology, Southwest Petroleum University, Chengdu 610500, China; Shandong Provincial Key Laboratory of Depositional Mineralization & Sedimentary Mineral, Shandong University of Science and Technology, Qingdao 266590, China; State Key Laboratory of Oil and Gas Reservoir Geology and Exploitation, Southwest Petroleum University, Chengdu 610500, China, e-mail: wufengzh@swpu.edu.cn, e-mail: wfswpu2011@gmail.com
Cong Yao: School of Geoscience and Technology, Southwest Petroleum University, Chengdu 610500, China, e-mail: 1135876713@qq.com
Linlin Cong: Geological Research Institute (Karamay Mud Logging Company), Xibu Drilling Engineering Company Limited, China National Petroleum Corporation, Karamay 834000, China, e-mail: 941624080@qq.com
Yanping Xi: School of Geoscience and Technology, Southwest Petroleum University, Chengdu 610500, China, e-mail: 1649174304@qq.com

Open Access. © 2020 Feng Wu *et al.*, published by De Gruyter. This work is licensed under the Creative Commons Attribution 4.0 Public License.

sandstone and shale [22]. With in-depth studies of the two-phase flow mechanism of rock, some researchers propose other pore-scale displacement experiment methods such as the slabbed core sample pore-scale displacement experiment and the microscopic glass etching displacement experiment [11–13]. These two alternatives are similar in terms of displacement and observation, but they vary in the objects (physical models) displaced and observed. In the slabbed core sample based pore-scale displacement experiment, the core sample is cut into thin sections before displacement and observation. Such an easy, cost-effective technique can maintain the pore structure characteristics and wettability of the rock. However, the model is so opaque that it is hard to observe the pore-scale two-phase flow characteristics [11]. As for the microscopic glass etching displacement experiment, displacement and observation are done on a transparent micropore network model made of thin sections. Such a model is highly visualizable so that we can directly look into the pore-scale dynamic flow characteristics. Therefore, it is widely used in the research on the mechanism of displacement of oil by water [12,13]. In the past few years, a great many researchers have made fruitful achievements in the theories and technologies of the pore-scale displacement experiment [11–15]. With regard to the core plug displacement experiment and the microscopic glass etching displacement experiment, researchers have not only successfully observed the two-phase flow characteristics under a microscope but also attempted to perform quantitative analyses of the parameters of two-phase flow.

In recent years, with the improvement of pore-scale flow theories and computer performance, the numerical simulation of pore-scale flow in rock has developed rapidly [15–19]. At present, the commonly used simulation methods include the Lattice Boltzmann Method (hereafter referred to as "the LBM") [23–27] and the Navier–Stokes equation based numerical simulation method [28–35]. Both methods are based on the pore network characteristics and used to simulate the pore-scale fluid flow in rock. Originating in the mid-1980s, the LBM is a flow-field simulation method developed from lattice gas automaton, which adopts the discrete media model to simulate fluid movement. By contrast, the numerical simulation method based on Navier–Stokes equations takes the fluids as an uninterrupted entirety and calculates the parameters of movement by means of calculus. To be specific, it includes the finite difference method (hereafter referred to as "the FDM") [31] and the finite element method (hereafter referred to as "the FEM") [32–35]. Generally, the FDM is based on differential equations. After discretizing the problem's domain, this method replaces the difference and difference quotient with differential and differential quotient approximations, through which the differential equation and boundary conditions are solved, which can be concluded as solving a system of linear equations. The FDM is visualizable and allows easy meshing, but under some circumstances it is inapplicable to a sophisticated boundary. Given this deficiency, the FDM is almost replaced by the FEM, which is more flexible in meshing and more applicable to boundaries. Consequently, the FEM is broadly applied in the simulation of fluid flow [32–35].

To a large extent, the existing studies of pore-scale two-phase flow in rock focus on oil–water flow. There are insufficient studies on pore-scale gas–water two-phase flow. Moreover, it is uncertain whether physical experimental observation or numerical simulation is appropriate for the research. Using the same micro-pore network model, we studied the characteristics of pore-scale gas–water two-phase flow with the microscopic glass etching displacement experiment and the Navier–Stokes equation based FEM, respectively. Next, we contrasted the advantages and disadvantages of the two methods in hopes of providing reference for the studies of the mechanism of pore-scale gas–water two-phase flow in rock and the effective development of gas reservoirs.

2 Methods

2.1 Glass etching displacement experiment

2.1.1 Preparation of the glass etching model

This research constructed the glass etching model based on the images of thin sections, and the procedure is as follows (Figure 1): first, convert the image of thin sections (Figure 1a) to a gray scale image (Figure 1b) via ImageJ software; second, segment the gray scaled thin section image into pores and grains (Figure 1c) via Avizo software, i.e., the pore network image is obtained; third, draw an image for the glass etching model in accordance with the segmentation via Coreldraw software (Figure 1d); fourth, etch the image on glass to create a glass etching model (Figure 1e). The preparation craft (especially photolithography) greatly determines the precision of the model and further impacts the results of the following displacement experiment. Now, photolithography is mainly applied in the photoelectric technology but seldom seen in oil–gas resource development. Some researchers have done

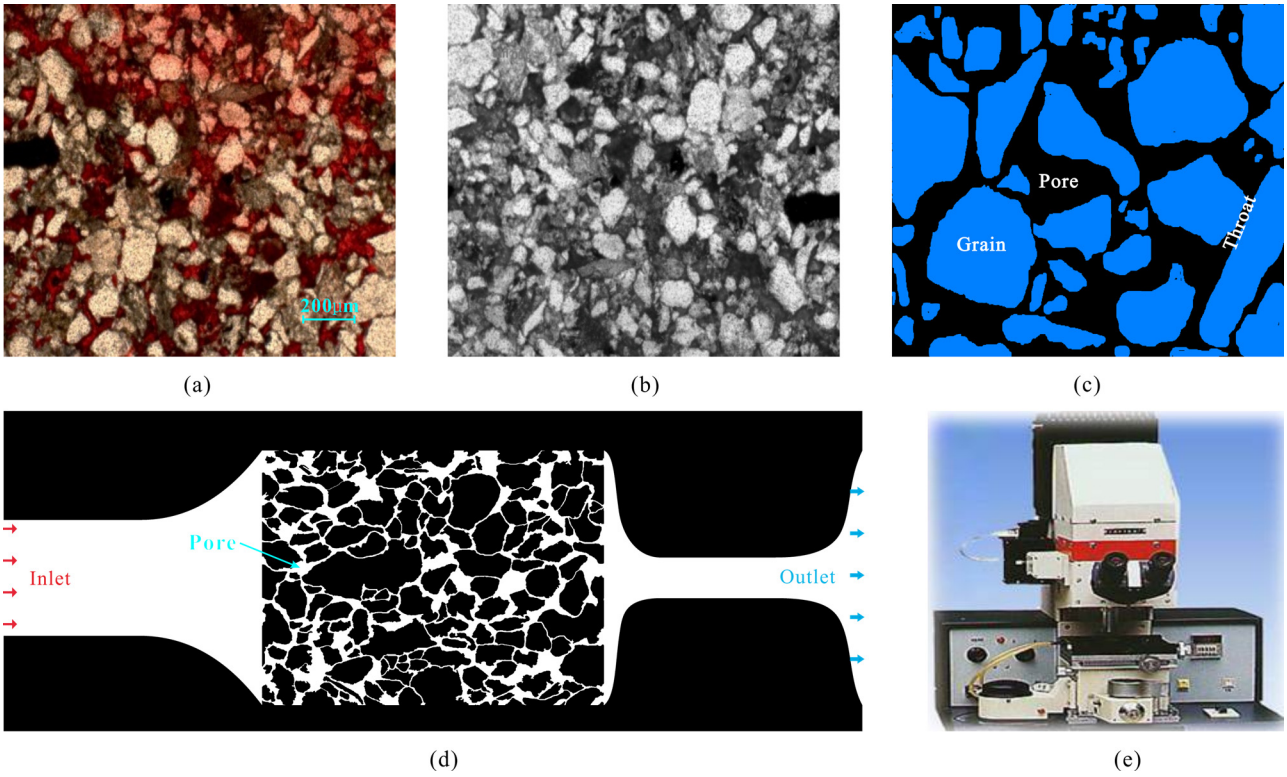

Figure 1: Schematic diagram of the preparation of the glass etching model. (a) Thin section image, (b) gray-scale image, (c) pore space after segmentation, (d) image for glass etching, (e) glass etching.

in-depth research on the theories and technologies of microscopic glass etching model preparation, which offers theoretical guidance to the research on pore-scale flow. In detail, there are three steps in the preparation of a micro glass etching model: (1) washing and glue mixing. Open the vacuum pump and suck the washed glass sheet; drip a few primer molecules on the sheet as a tackifier; dry the sheet for 10 min before coating it with a photoresist and lay the mixture aside for 30 s before a film of certain thickness is formed. Here, the mixture of primer and photoresist can prevent shallow nicks and the deformation of V-shape slots on the pore. (2) Exposure and development. Dry the sheet in advance for 10 min before exposure; expose the sheet to a lithography machine for 80–120 s; dip the exposed sheet in a photographic developer for 5 min; and then dry it for 10 min. (3) Etching and glue removal. Dry and wax the sheet and then etch it in acid for 5–15 min; dissolve the exposed photoresist, and the etching model is formed.

2.1.2 Glass etching displacement experiment

Currently, most of the microscopic glass etching displacement experiments focus on oil–water two-phase flow. Due to the great difference in the colors of oil and water, the experiment process can be observed clearly [36,37]. In terms of the research on gas–water two-phase flow, the colors of gas and water are similar, making it hard to observe the interface of gas and water. In this research, to have a better look at the displacement experiment process, methylene blue is used to dye the water so as to distinguish it from the gas (nitrogen). The experiment can be started after the displacement model and the displacing fluid are ready. The experimental device is shown in Figure 2, and here are the specific steps: (1) install and fix the micro glass etching model, exert adequate confining pressure on the model and vacuumize it, then fill the model with water (dyed with methylene blue) from the inlet until the model is saturated. (2) At a temperature of 24°C, turn on and set the micro constant-speed pump at a preliminary displacement velocity of 0.05 mL/min, and then fill the pores with gas (nitrogen) continuously (20 min). (3) When the gas–water distribution reaches a stable status, increase the flow velocity from the inlet gradually and displace the model, respectively, at flow velocities of 0.1 mL/min for 20 min, 0.2 mL/min for 10 min and 0.5 mL/min for 5 min until no water runs out from the outlet; at this time, the displacement is finished. A Zeiss SteREO Discovery.V12 micro camera with a total magnification of 12×–375×, accuracy of

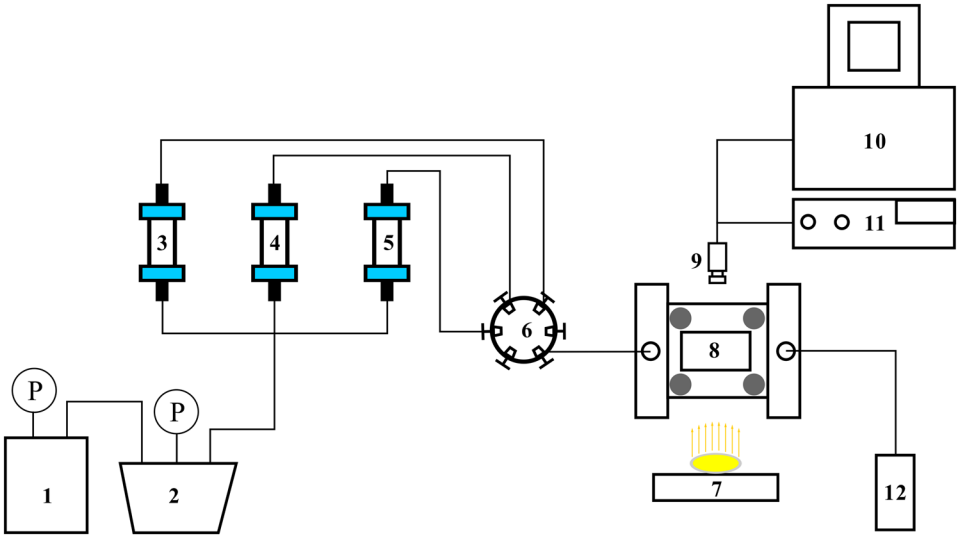

Figure 2: Schematic diagram of the glass etching based gas–water flow experimental device. (1) Air compressor; (2) pressure buffer tank; (3–5) containers; (6) six valve; (7) light; (8) micro-model and holder; (9) camera; (10) computer; (11) video system; (12) liquid loading container.

focusing of 350 nm and field of view of 2.3–28.8 mm is used to record the whole experiment.

2.1.3 Processing and analysis of displacement images

Displacement images at different stages can be produced using image processing software. In order to differentiate the two-phase interface and analyze the seepage characteristics, the images should be further processed (Figure 3): first of all, import the displacement images to ImageJ software and convert them to gray scales; then, import the gray scales to Avizo software and segment them, while, the pore spaces occupied by gas and water, respectively, were filled with different colors.

2.2 Finite element numerical simulation

2.2.1 Finite element model construction

The first two steps of the two-dimensional finite element model construction (Figure 4) are the same as those for the glass etching model construction: the image of the thin section (Figure 4a) is converted to a gray scale image (Figure 4b) and then segmented (Figure 4c). Then, the third step is to construct a full-size pore network model based on the segmented pore network image (Figure 4d). Fourth, the pore network model is imported to the COMSOL Multiphysics software to define a solution domain (Figure 4e). In this model, the inlet is on the left while the outlet is on the right, and the closed curved areas represent the granules while other connected areas are pores and throats that are set as the solution domain. Fifth, the solution domain is meshed by using free triangles (Figure 4f); the grids at the throats are dense while the ones among the pores are sparse. Also, the closer to the pore wall the grids are, the denser they are.

2.2.2 One-phase flow simulation

One-phase flow in rock can be seen as creeping flow. The main task of the two-dimensional one-phase flow simulation is to solve the Stokes equations. Due to the small size of the model, it is regarded that during the simulation, the fluid in the pores is at constant temperature with the same density, so, suppose that the fluid is incompressible and the gravity can be ignored. The inlet is on the left while the outlet is on the right, and under constant pressure, the fluid enters from the inlet. Here, the Stokes equations and the continuity equations of the one-phase flow can be expressed as follows:

$$\nabla\cdot[-pI + \mu(\nabla u + (\nabla u)^{\mathrm{T}})] = 0 \tag{1}$$

$$\nabla\cdot(u) = 0, \tag{2}$$

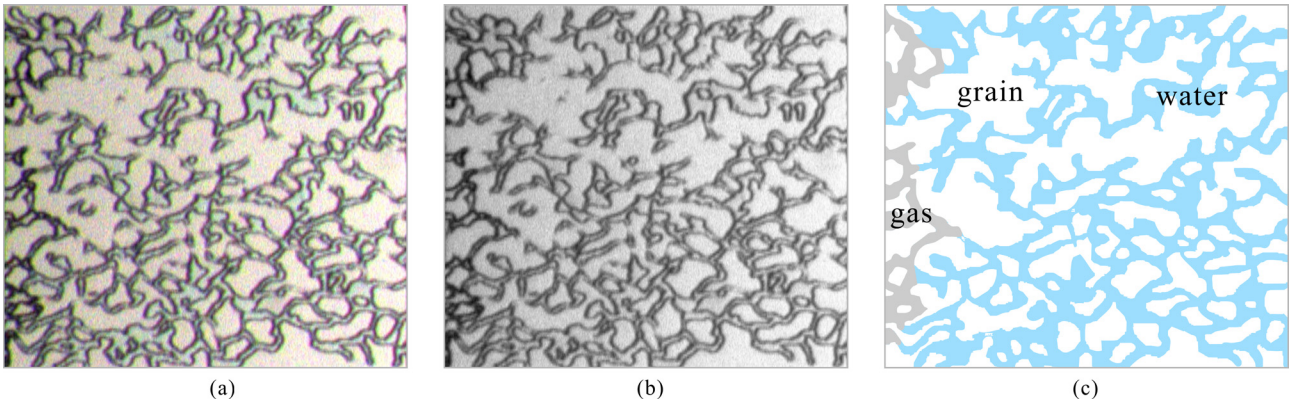

Figure 3: Schematic diagram of displacement image processing. (a) Initial image after displacement, (b) gray-scale image, (c) image after gas and water identified.

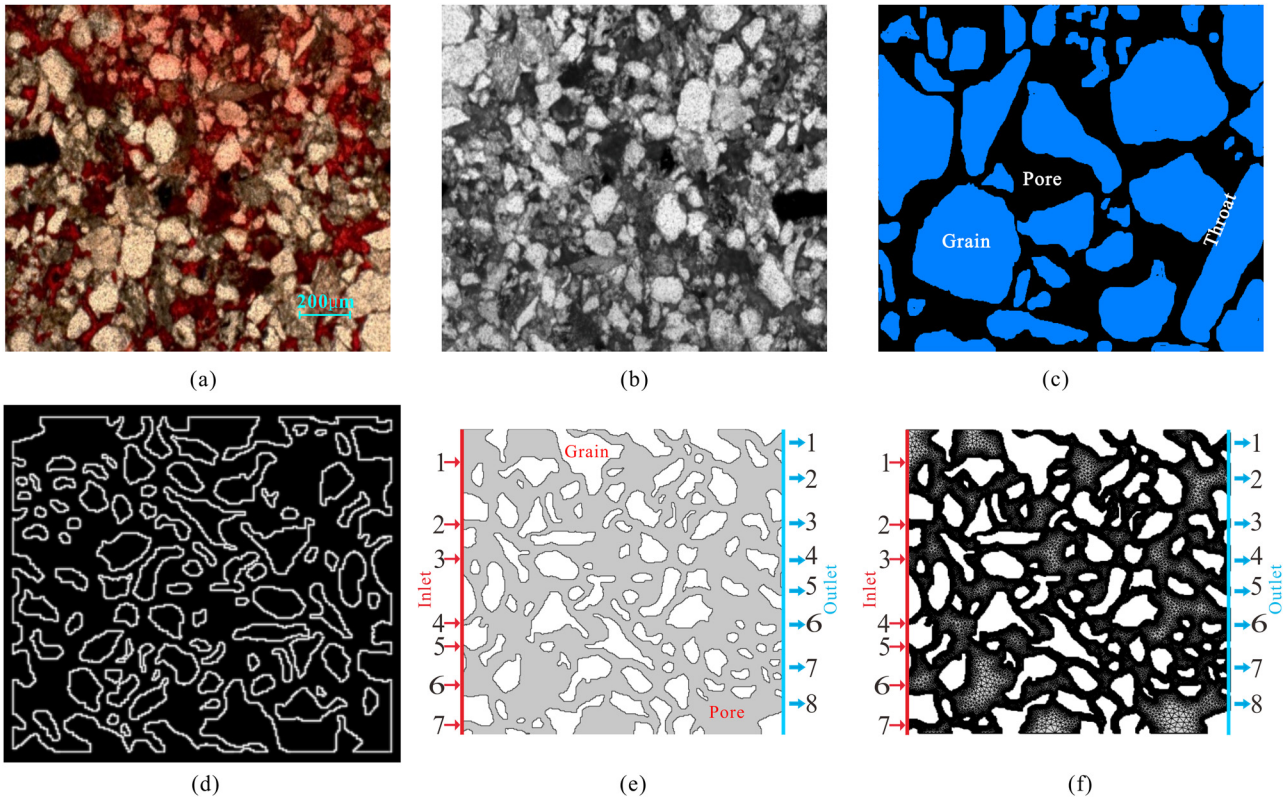

Figure 4: Schematic diagram of displacement image processing. (a) This section image, (b) gray-scale image, (c) pore space after segmentation, (d) pore structure model, (e) solution domain, (f) mesh generation.

where P is the pressure, Pa; I is the unit matrix; μ is the fluid viscosity, Pa s; u is the velocity vector, m/s; and T is the absolute temperature (293.15 K).

The boundary conditions are as follows: the pressure of the inlet at each pore of the model is equivalent and constant, so is that of the outlet at each pore. There is no inflow or outflow except for the flows from the inlet and the outlet. The pore wall is intermediately wet, and the normal component of the flow rate in the direction of the pore wall is zero.

2.2.3 Gas–water two-phase flow simulation

Two-phase flow in rock can be seen as laminar two-phase flow. In the gas–water two-phase numerical simulation,

the mathematical model is constructed through the Navier–Stokes equations combined with the level set method. The equations are solved using the FEM. In this model, the specified Material 1 (wetting phase) is water, which saturates the pores and throats, and Material 2 (non-wetting phase) is gas. The gas enters the inlet from the left and displaces the water in the pores, and the water runs out from the outlet. The level set function φ defines the volume fractions of the gas and the water, respectively. For water, $\varphi = 0$. For gas, $\varphi = 100\%$. Besides, the two-phase interface is traced with the φ value of the initialized level set functions in order to study the dynamic characteristics of the gas–water two-phase interface. The dynamic equation of the gas–water two-phase interface can be expressed as follows:

$$\frac{\partial \varphi}{\partial t} + u \cdot \varphi = \gamma \nabla \cdot (\varepsilon \nabla \varphi - \varphi(1 - \varphi)) \frac{\nabla \varphi}{|\nabla \varphi|}, \tag{3}$$

where φ is the level set function; t is the two-phase displacement time, s; γ is the initialized parameters (the default value is 1 m/s); and ε is the parameter of interface thickness (the default value is $h_{\max}/2$, $h_{\max}$ is the largest grid unit of the two-phase interface flowing area).

Apart from defining the flow interface, the level set function φ can also express the flow characteristics (the jumps of density and viscosity), i.e.,

$$\rho = \rho_{\text{air}} + (\rho_{\text{water}} - \rho_{\text{air}})\varphi \tag{4}$$

$$\mu = \mu_{\text{air}} + (\mu_{\text{water}} - \mu_{\text{air}})\varphi, \tag{5}$$

where ρ is the density, kg/m^3; ρ_{water} and ρ_{air} are, respectively, the density of water and the density of gas, kg/m^3; μ_{water} and μ_{air} are, respectively, the dynamic viscosity of water and the dynamic viscosity of gas, Pa s.

Compared with the sound velocity, the fluid velocity is so low that it can be ignored. Therefore, we can suppose that water and gas are incompressible. The Navier–Stokes equations can express the mass and momentum transfer of the incompressible two-phase flow. Taking the interfacial tension into consideration, the Navier–Stokes equations and the continuity equations of the two-phase flow can be expressed as follows:

$$\rho \frac{\partial u}{\partial t} = \nabla \cdot [-pI + \mu(\nabla u + (\nabla u)^{\text{T}})] + \rho g + F_{\text{st}} \tag{6}$$

$$\nabla \cdot u = 0, \tag{7}$$

where I is the unit matrix; g is the gravity, N/m; F_{st} is the gas–water interfacial tension, N/m.

The interfacial tension of the two-phase flow can be expressed as follows:

$$F_{\text{st}} = \nabla T \tag{8}$$

$$T = \sigma(I - nn^{\text{T}})\delta, \tag{9}$$

where σ is the interfacial tension coefficient, N/m; n is the perpendicular unit vector to the interface; and δ is the Dirac delta function on the interface, $1/m$.

The perpendicular unit vector to the interface is

$$n = \frac{\nabla \varphi}{|\nabla \varphi|}. \tag{10}$$

The Dirac delta function δ can be approximated according to the following smooth function:

$$\delta = \text{Б}\, |\nabla \varphi| |\varphi(1 - \varphi)|. \tag{11}$$

3 Geological setting

The western Sichuan depression is located in the western part of the Sichuan Basin, on the northwestern margin of the Yangtze Plate, and adjacent to the Longmenshan nappe tectonic belt in the west. The western Sichuan depression entered the foreland basin development stage from the end of the Late Triassic and deposited a thick Triassic–Jurassic–Cretaceous terrigenous clastic strata. A large number of tight gas reservoirs have been found in the Triassic Xujiahe Formation, the Shaximiao Formation and the Penglaizhen Formation in the Jurassic [38]. The study area of this research is the Majing–Shifang–Xinchang contiguous structure and the object of the study is the tight sandstone reservoirs of the Shaximiao Formation and the Penglaizhen Formation in the Jurassic (Figure 5). The tight sandstone reservoirs of the Penglaizhen Formation in western Sichuan can be divided into three categories according to their physical properties and pore structure types (Figure 6): the type I reservoir features porosity > 11%, permeability > 0.8 mD and a bimodal distribution shown in NMR. The movable peak amplitude is high, and the mercury intrusion displacement pressure is lower than 0.3 MPa (Figure 6a). The type II reservoir has a porosity of 9%–11% and a permeability of 0.1–0.8 mD. The NMR shows a bimodal distribution with a moderate peak amplitude and a displacement pressure of 0.3–1.0 MPa (Figure 6b). The type III reservoir has a porosity of 6%–9% and a permeability of 0.03–0.10 mD. The bimodal distribution in NMR is not obvious, the movable peak amplitude is low and the mercury intrusion displacement pressure is 1–2 MPa (Figure 6c). A photograph of a typical cast thin section was selected for each type I reservoir, type II reservoir and type III reservoir. At the same time, a glass etching

displacement experiment, a single-phase flow simulation and a gas–water two-phase flow simulation were performed.

4 Results

4.1 Results of the glass etching displacement experiment

In the microscopic glass etching displacement experiment, three cast thin sections with different types of pore structures were used to make glass etching models and to conduct the gas displacing water experiment. The micro glass etching models were manufactured in the State Key Laboratory of Oil and Gas Reservoir Geology and Exploitation, Southwest Petroleum University. If the primer and photoresist were not spread evenly over the glass, or the thicknesses of the primer film and photoresist film were not suitable, the pore space in the etching model may not match the pore network image well. In this research, the success rate of the manufacturing of the micro glass etching model is 75%. The gas–water two-phase flow characteristics and the distribution law of gas and water after displacement were studied. In the initial stage of

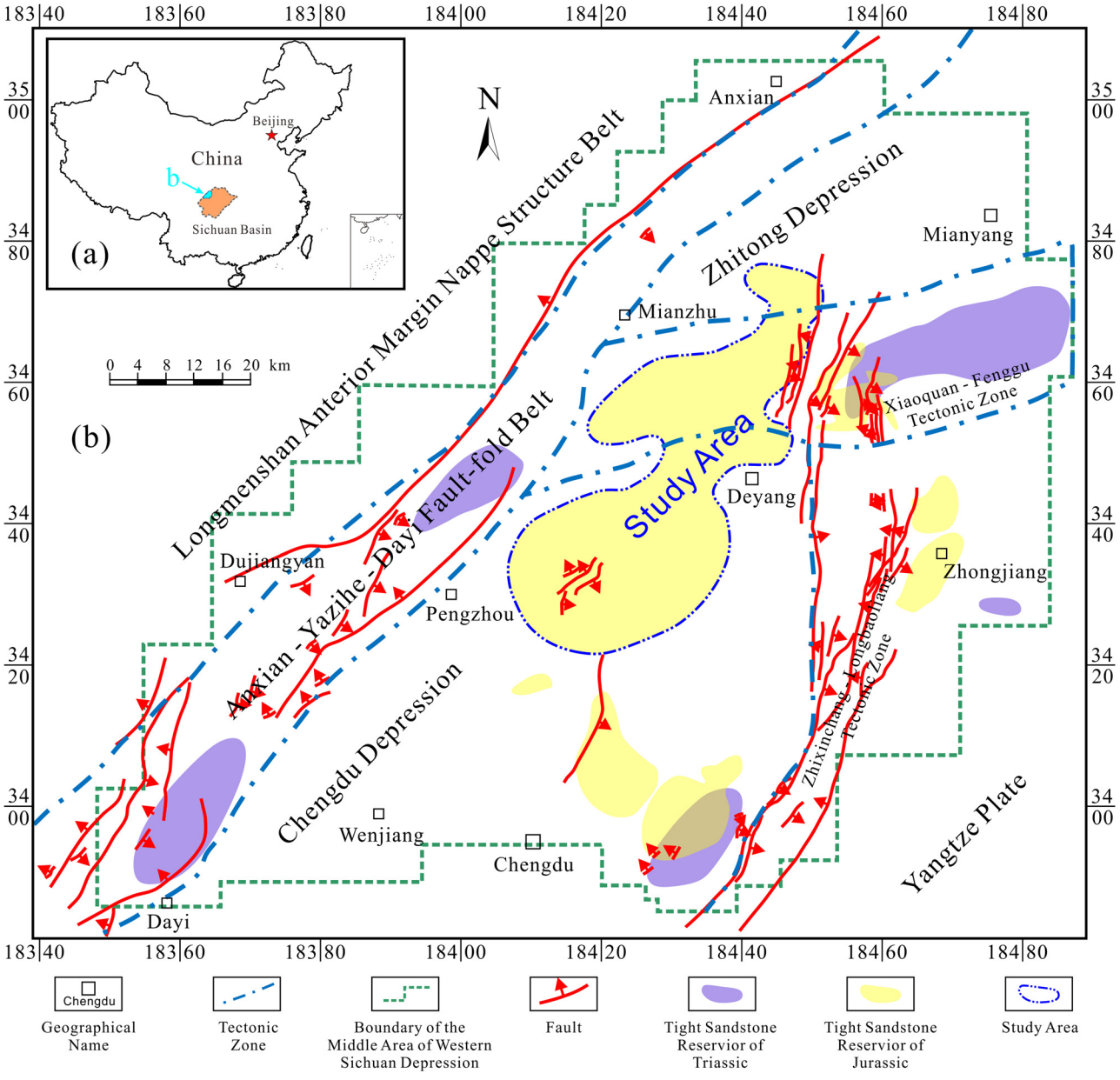

Figure 5: Geological structure map of the study area. (a) The location of the Sichuan Basin on the map of China, (b) the study area is the Majing–Shifang–Xinchang contiguous structure in the western Sichuan depression.

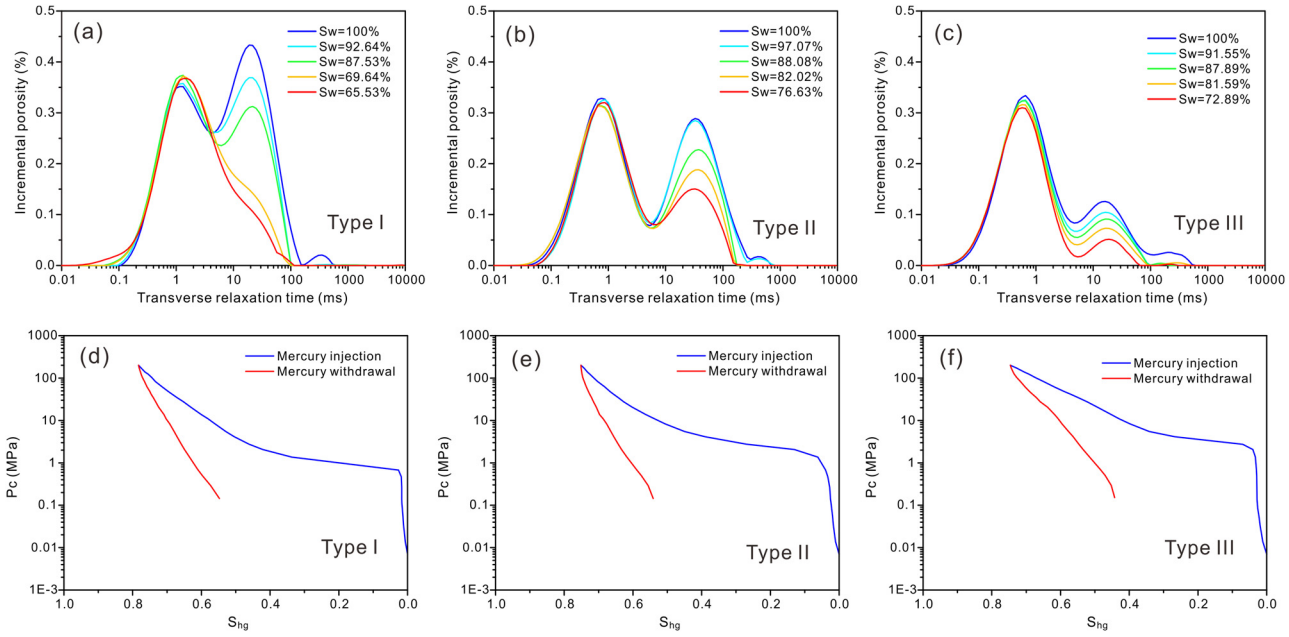

Figure 6: Pore structure characteristics of type I, type II and type III tight sandstone reservoirs. (a, b, c) T2 distribution of type I, type II and type III tight sandstone reservoirs respectively. From type I to type III, the amplitude of the right peak decreases. (d, e, f) Mercury injection curve of type I, type II and type III tight sandstone reservoirs respectively. From type I to type III, the capillary pressure (Pc) increases.

the glass etching gas displacing water experiment, the water saturated the pore space, and all three models had the left end as the inlet and the right end as the outlet. The gas was injected into the model from the left end inlet for the displacement experiment, and as the experiment went on, the water flowed out from the outlet. The basic parameters of gas and water are listed in Table 1.

In the gas displacing water experiment, due to the anisotropy of the radius of the pores and throats, different pore throat radii have different capillary pressures, the capillary resistance of the gas displacement is different and the speed of the displacement front edge is different. There is a significant pore-scale finger-like breakthrough. That is, under the circumstance of the gas being injected into the model from the left end inlet, if the displacement pressure is greater than the capillary resistance of the throat, the gas passes through the throat first; if the displacement pressure is less than the capillary resistance, the gas first stops moving forward for a period of time, and then a migration jump occurs. The displacement front edge advances along the connected path with less capillary resistance and reaches the outlet first to form a dominant channel. When the gas reaches the outlet, most of the injected gas flows along the dominant channel. As shown in Figure 7, the displacement front edge of the type I reservoir advances more evenly, the phenomenon of a finger-like breakthrough is weaker and the displacement effect is better. When the gas is at the outlet of the type II reservoir model, the water saturation is 56.87% and the final water saturation is 52.29%. When the gas is at the outlet of the type III reservoir model, the water saturation is 57.80%, the final water saturation is 46.25%, the water saturation decreases less, the displacement effect is not favorable and the finger-like breakthrough is obvious. At the end of the glass etching displacement experiment, it can be observed that the trapped water is mainly distributed in the small pores, large pores and the end of the pores controlled by the small throats.

4.2 Results of the finite element numerical simulation

4.2.1 Results of the single-phase flow simulation

The dimensions of the constructed type I, II and III reservoir models are 11.70 mm × 10.98 mm, 11.76 mm × 10.97 mm and 12.21 mm × 10.93 mm, respectively. In the numerical simulation of single-phase flow, gas is injected into the pore space

Table 1: Parameters of gas and water

Fluid	Density, kg m^{-3}	Dynamic viscosity, Pa s	Temperature, K
Water	1.0×10^3	1.0×10^3	293.15
Gas	0.8	17.58×10^{-6}	293.15

from the inlet of the model under constant pressure conditions. As shown in Figure 8a–c, the pressure of the gas in the model gradually decreases from the left (inlet) to the right (outlet). Due to the different pore structures of the three types of reservoir models, the capillary resistance and the pressure contour distribution are also different. In the type I reservoir model, the area with a pressure greater than 0.67 kPa is larger, the area with a pressure of 0.57–0.67 kPa is larger in the type II reservoir model and the area with a pressure of 0.26–0.57 kPa is larger in the type III reservoir model. The type I reservoir model has a larger pore radius than type II and type III, and therefore, its pressure decreases at the slowest speed along the displacement direction. As shown in Figure 8d–f, in the flow rate diagram, blue indicates a low flow velocity and red indicates a high flow velocity. The flow rate at the center of the channel is quicker than that of the inlet, and it becomes slower when approaching the pore wall. The type I reservoir model has the largest pore throat radius, so the capillary resistance is the smallest and the flow rate is the quickest.

4.2.2 Results of the gas–water two-phase flow simulation

In order to compare with the microscopic glass etching displacement experiment easily, the numerical simulation of gas–water two-phase flow adopts the same pore

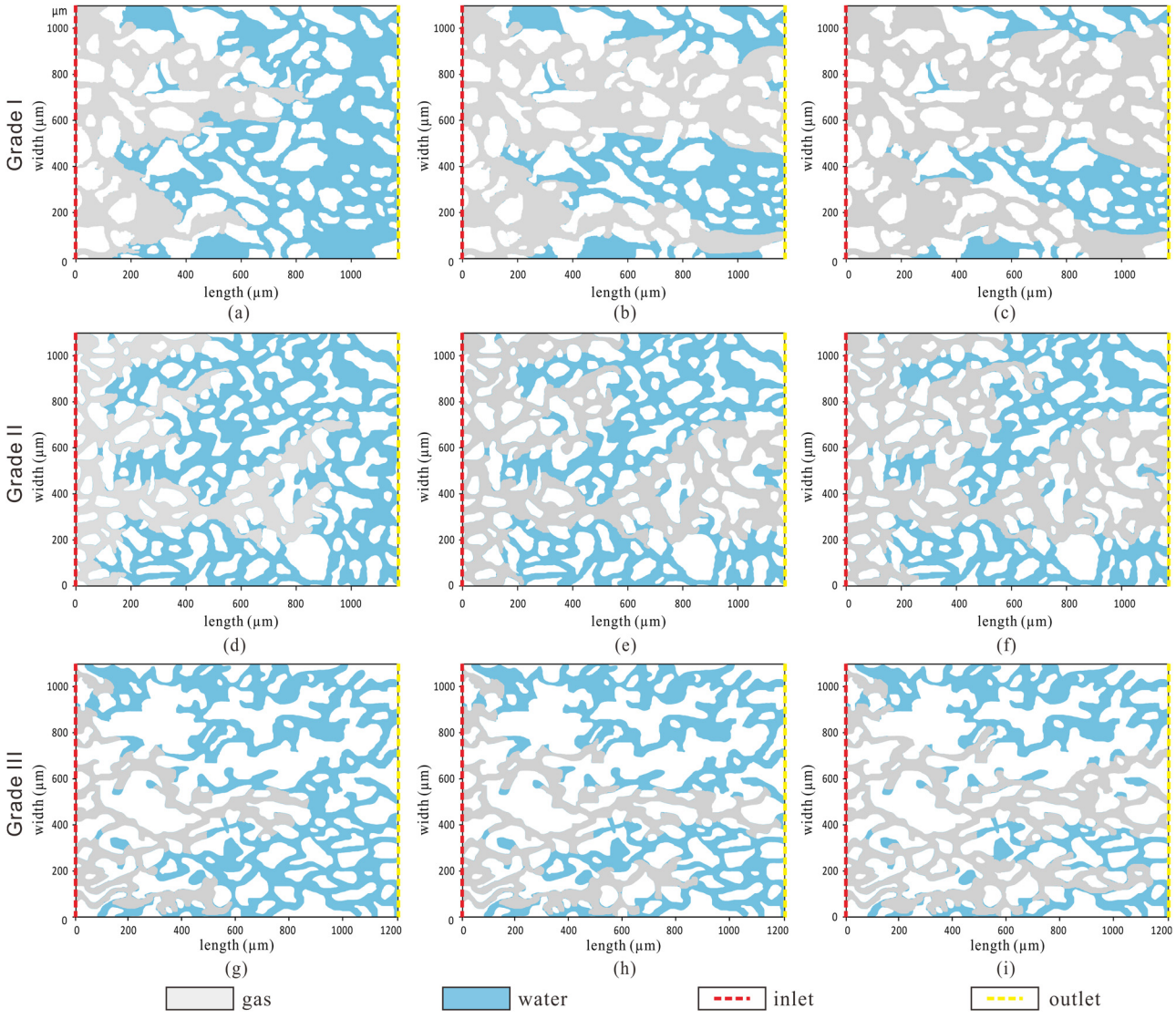

Figure 7: Glass etching based experimental results of gas–water flow of type I, type II and type III reservoir models. (a) Sw = 62.1%, (b) Sw = 34.6%, (c) Sw = 18.61%, (d) Sw = 74.31%. (e) Sw = 56.87%, (f) Sw = 52.29%, (g) Sw = 70.68%, (h) Sw = 57.80%, (i) Sw = 46.25%.

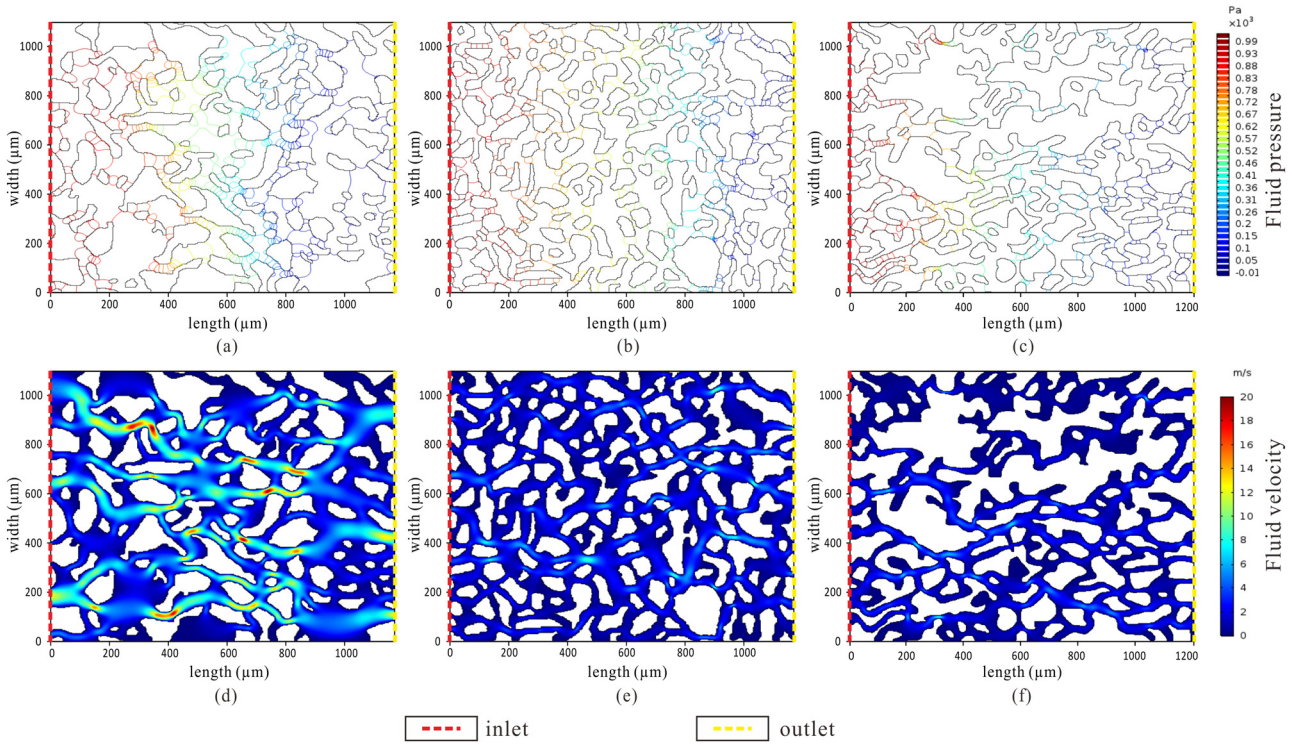

Figure 8: Simulation results of one-phase flow of type I, type II and type III reservoir models. (a) Fluid pressure of type I reservoir model, (b) fluid pressure of type II reservoir model, (c) fluid pressure of type III reservoir model, (d) fluid velocity of type I reservoir model, (e) fluid velocity of type II reservoir model, (f) fluid velocity of type III reservoir model.

network model as the microscopic glass etching displacement experiment. The conditions of the inlet and outlet, and parameters of gas and water used in the model of numerical simulation remain consistent with the microscopic glass etching displacement experiment. The related parameters of gas and water are listed in Table 1.

During the numerical simulation of gas displacing water, there is an obvious pore-scale finger-like breakthrough, that is, the gas moves forward with less resistance along one or more continuous paths composed of large throats and connected pores and reaches the outlet first (Figures 9–11). In the initial stage of the simulation, the gas is injected from the left end (inlet). When the displacement front edge reaches the right end (outlet) of the model, the water saturation of the type I, II and III reservoirs in the model is 34.69% (Figure 9c), 56.87% (Figure 10e) and 57.80% (Figure 11e), respectively. The type I reservoir model has a larger pore throat radius than type II and type III, and it adopts less displacement time. When the front edge of the two-phase flow interface reaches the outlet, the displacement range continues to increase (Figure 9). Because the pore throat radii of the type II and type III reservoir model are small, the resistance of the capillary is large, and the displacement resistance in the flow channel reduces after the gas reaches the outlet of the model. At this time, the injected gas basically moves along the dominant channel, the scope of the displacement is no longer expanded, the displacement efficiency is basically no longer increased, and the phenomenon of a finger-like breakthrough becomes more obvious (Figures 10 and 11).

5 Discussion

5.1 Influence of pore structure on gas–water flow characteristics

There is an obvious finger-like breakthrough in the microscopic glass etching displacement experiment and the gas–water two-phase flow numerical simulation, that is, when the gas flows in the rock, due to the anisotropy of the pore structure, the gas front edge encounters pore throats of different radii and different capillary resistances. When the displacement pressure is greater than the pore throat capillary resistance, the gas passes first; in the opposite case, the gas stops for a while and then

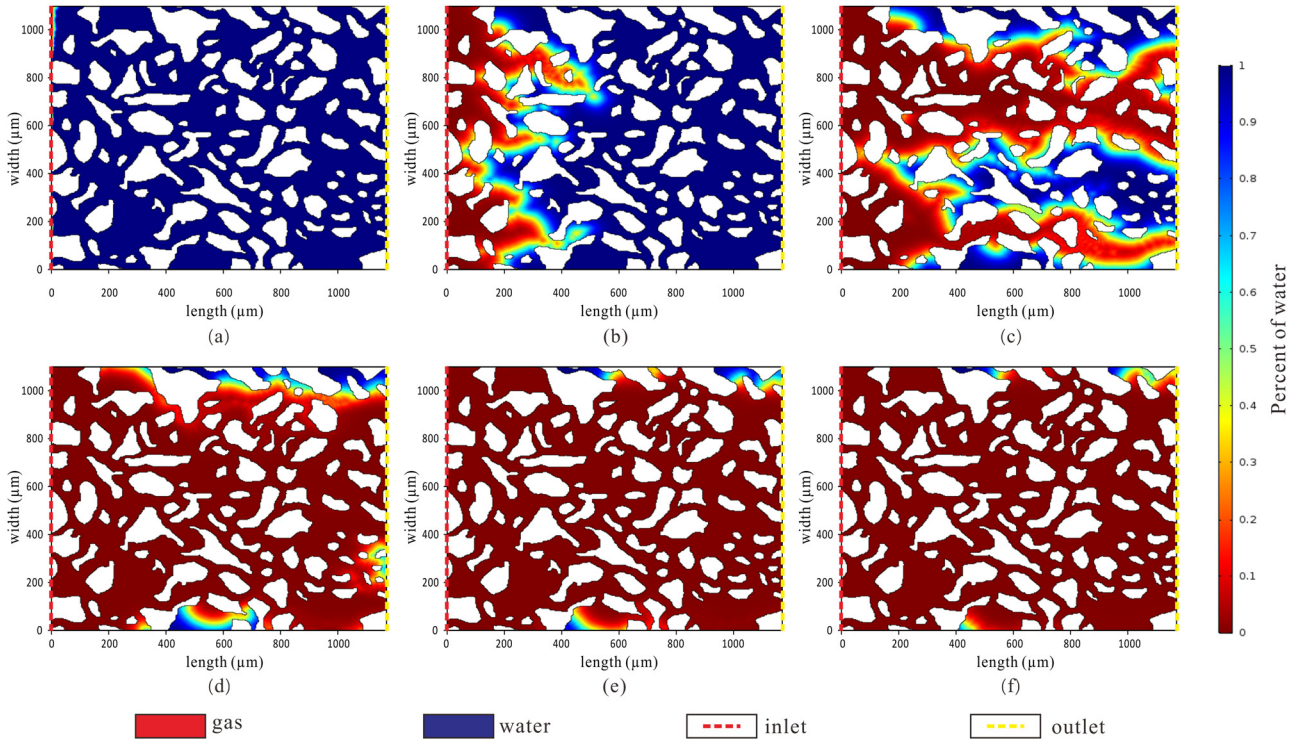

Figure 9: Simulation results of gas–water flow of the type I reservoir model. (a) t = 0 ms, Sw = 100%; (b) t = 0.04 ms, Sw = 76.70%; (c) t = 0.08 ms, Sw = 34.69%; (d) t = 12 ms, Sw = 6.44%; (e) t = 16 ms, Sw = 2.37%; (f) t = 20 ms, Sw = 1.32%.

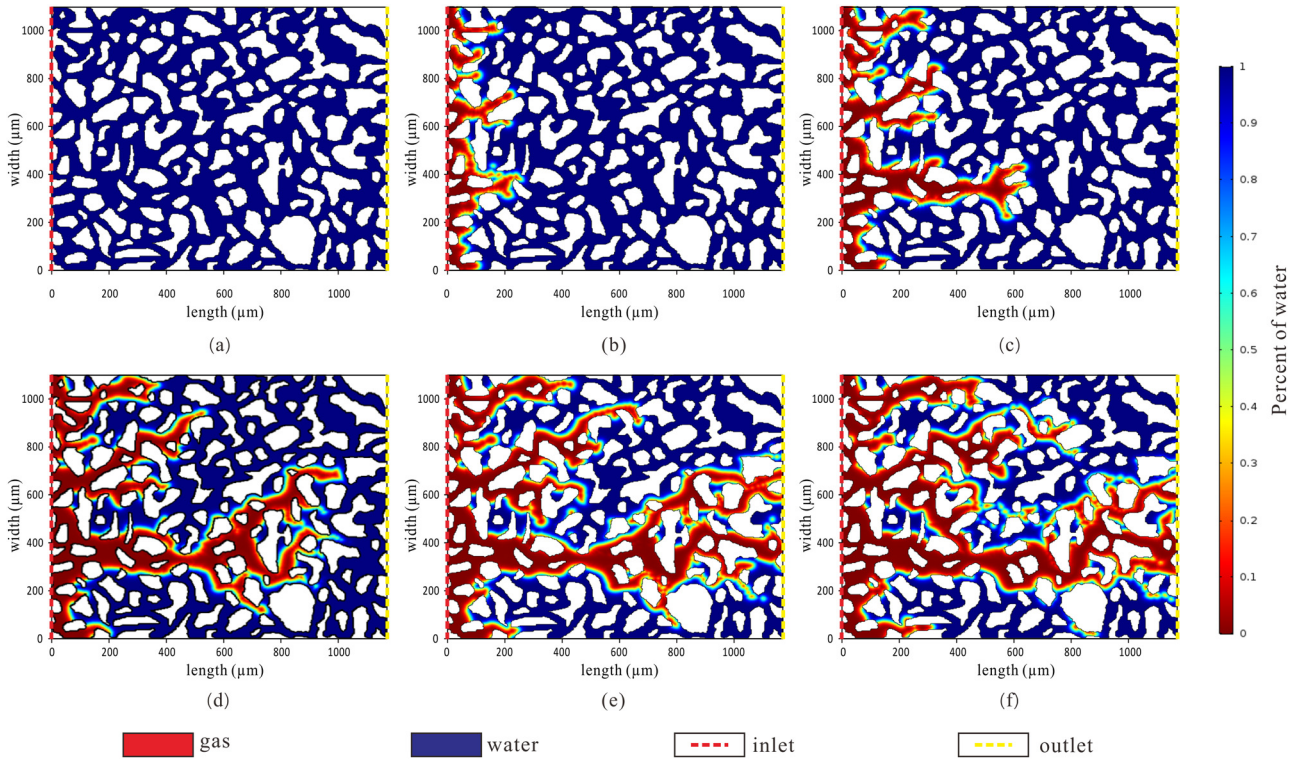

Figure 10: Simulation results of gas–water flow of the type II reservoir model. (a) t = 0 ms, Sw = 100%; (b) t = 0.04 ms, Sw = 90.12%; (c) t = 0.08 ms, Sw = 80.30%; (d) t = 12 ms, Sw = 65.23%; (e) t = 16 ms, Sw = 56.87%; (f) t = 20 ms, Sw = 52.29%.

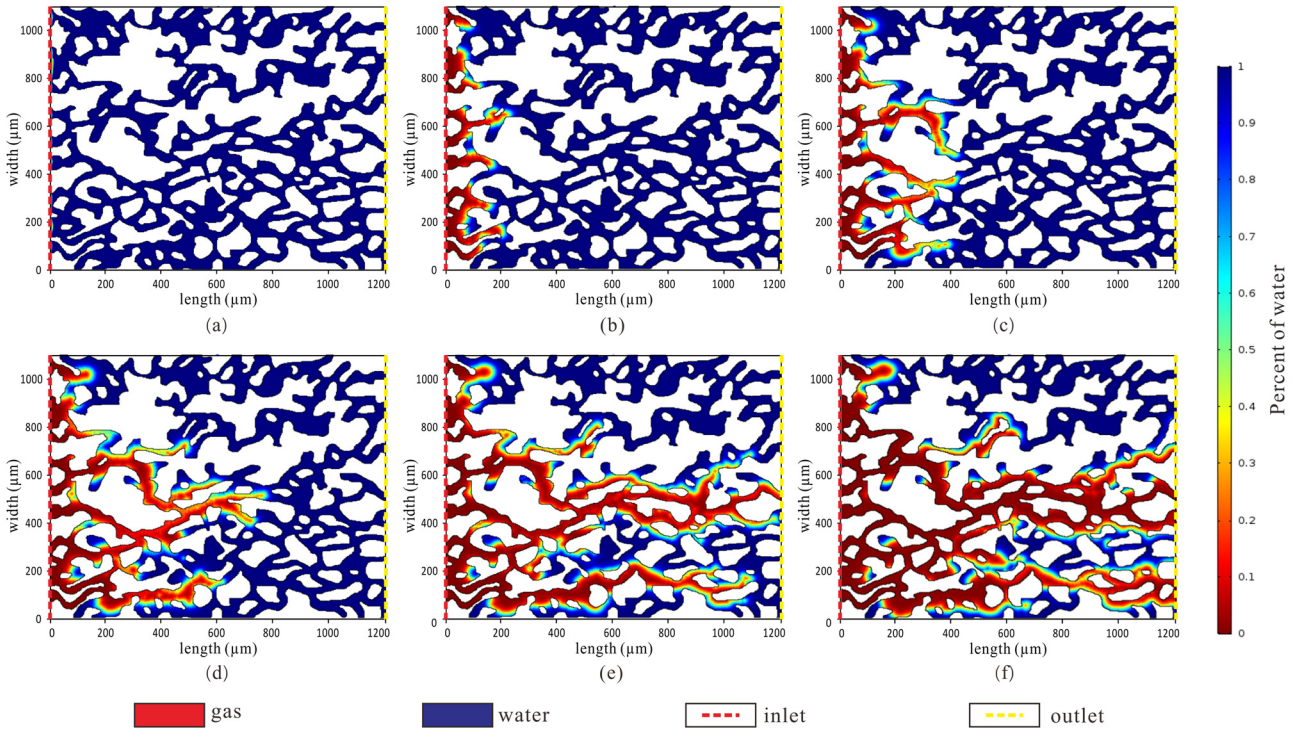

Figure 11: Simulation results of gas–water flow of the type III reservoir model. (a) t = 0 ms, Sw = 100%; (b) t = 0.04 ms, Sw = 96.96%; (c) t = 0.08 ms, Sw = 83.79%; (d) t = 12 ms, Sw = 73.94%; (e) t = 16 ms, Sw = 57.80%; (f) t = 20 ms, Sw = 46.25%.

jumps forward. As the displacement pressure continues to increase, the pause time in the middle of this jump is gradually reduced. Meanwhile, in reservoirs with different pore structure types, the duration for which the gas stays at the small throats is different. The pause time in the small throats of the type III reservoir is significantly longer than that of the type I reservoir and the type II reservoir. This is because the type I and II reservoirs have larger throat radii and higher permeability, while the type III reservoir has smaller throat radii and a lower permeability. The type III reservoir has smaller throat radii and greater capillary pressure compared with the type I and II reservoirs (Figure 6), and thus the gas needs greater pressure to move forward again. Therefore, the speed at which the gas front edge advances is inconsistent, that is, a viscous finger-like breakthrough similar to a tree-like shape appears (Figures 7 and 9–11). As the displacement pressure increases, the tree-like shape becomes more pronounced. After the gas displacing water process is completed, the water distributed in the large pore throats and in the pores connected to large pore throats is displaced, and the trapped water is mainly distributed in the flow area of the high permeability pore, the pore area perpendicular to the fluid flow direction and the ends of the unconnected pores (Figure 12).

5.2 Comparison of the advantages and disadvantages of experimental and simulation methods

In order to compare the similarities and differences between the results of microscopic glass etching displacement experiments and finite element numerical simulation, the displacement time of both methods was normalized. Comparison of microscopic glass etching displacement experiments and finite element numerical simulation shows the following.

(1) The numerical simulation results after normalization are basically consistent with the results of the microscopic glass etching displacement experiment (Figure 12). Under the same water saturation conditions, the two-phase flow interface front edge between the numerical simulation and the glass etching displacement experiment is basically the same (Figures 7h and 11e). There is an obvious finger-like breakthrough in both methods. When the displacement front edge reaches the inlet of the model, the water saturation of type I, II and III reservoir models is 34.69%, 56.87% and 57.80%, respectively, which is basically consistent with the inflection point of the curve in Figure 12. In the numerical simulation and glass etching displacement

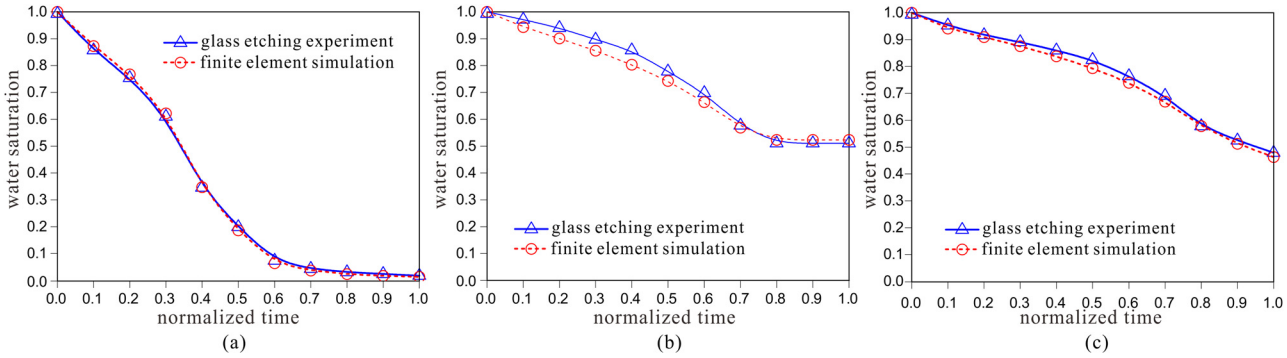

Figure 12: Trapped water induced by flow around, perpendicular pores and end of pores. (a) Grade I reservoir model, (b) grade II reservoir model, (c) grade III reservoir model.

experiment, the type I reservoir model has a larger throat radius and faster displacement time than the type II and type III reservoir models. When the front edge of the two-phase flow interface reaches the outlet of the model, the displacing efficiency and the displacement range of the type I reservoir model continue to increase, while they do not increase any more in the type II and type III reservoir models.

(2) Numerical simulation and glass etching displacement experiments are pore-scale visualization methods. The entire continuous displacement process can be directly observed through the glass etching displacement experiment, such as the migration jumps of gas as it passes through a narrow throat. The dynamic displacement characteristics at different moments can be better observed through numerical simulation. For example, in the initial stage of the displacement process, the gas first displaces the water distributed in the large throat and the pores connected to the large throat. After the displacement, the trapped water is mainly distributed in the small pores, large pores and pore ends controlled by the small throat (Figure 13).

(3) In the microscopic glass etching displacement experiment, we can better observe the migration and jumping phenomena of gas passing through the narrow throat, but this experiment is affected by unfavorable factors such as insufficient precision of the etching process and the instrument. This easily causes instability of the displacement pressure, and there is a certain error in the pore size and design size of the etched molding. On the whole, the glass etching model is characterized by high production cost, low model precision, easy deformation of the throat and low success rate, and thus the process technology needs to be further improved.

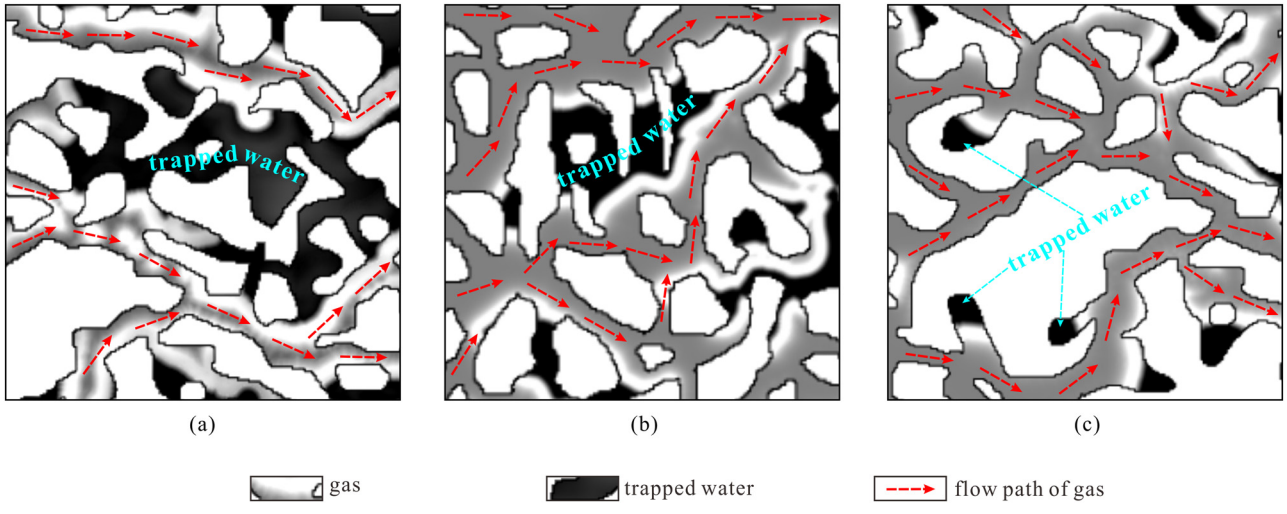

Figure 13: Comparison of water saturation of the glass etching experiment and the finite element simulation. (a) High permeability pores flow around induced trapped water, (b) pores perpendicular to the flow direction induced trapped water, (c) end of pores induced trapped water.

(4) The numerical simulation is not affected by unfavorable factors such as insufficient precision of the etching process and the instrument, and it can perfectly present the microscopic pore structure characteristics of the rock. However, the numerical simulation only considers limited boundary conditions, so it is impossible to accurately simulate some special pore-scale seepage phenomena. On the whole, the finite element numerical simulation method features simple operation, repeatability, strong computing power and low cost, and provides a new method for the study of pore-scale visualization of two-phase flow.

(5) At present, glass etching displacement experiments and finite element numerical simulations have their own advantages and disadvantages, and the combination of the two methods for the study of gas–water two-phase flow is favorable.

6 Conclusion

Based on the microscopic pore structure of rock, this study proposed a glass etching displacement technology based gas–water two-phase flow visualization experiment and a Navier–Stokes equation based finite element numerical simulation. When applying the same pore network model, the fluid displacement front edge morphology and seepage law obtained by these two methods are basically similar.

There is an obvious finger-like breakthrough in both the microscopic glass etching displacement experiment and the gas–water two-phase flow simulation. The water distributed in the large pores and large throats is displaced. The trapped water mainly exists in the area induced by flow around high-permeability pores, perpendicular pores and disconnected ends of pores (Figure 13). Through the microscopic glass etching displacement experiment, we can better observe the pore-scale finger-like breakthrough phenomenon and the migration and jumping phenomena of gas when passing through the narrow throat. However, when preparing the glass etching model, the pore throat is easily deformed and the success rate is too low. The finite element numerical simulation method has the advantages of easy operation, repeatability, strong experimental reproducibility and low cost, and provides a new choice for the study of pore-scale visualization of two-phase flow.

Acknowledgments: This research was supported by the Open Fund of State Key Laboratory of Oil and Gas Reservoir Geology and Exploitation (Southwest Petroleum University) (No. PLN201719), the Open Fund of Shandong Provincial Key Laboratory of Depositional Mineralization & Sedimentary Mineral (Shandong University of Science and Technology) (No. DMSM2018050) and the Scientific Research Starting Project of Southwest Petroleum University (No. 2017QHZ004).

References

[1] Avraam DG, Payatakes AC. Flow mechanisms, relative permeabilities, and coupling effects in steady-state two-phase flow through porous media. The case of strong wettability. Ind Eng Chem Res. 1999;38(3):778–86. doi: 10.1021/ie9804040.

[2] Wu M, Xiao F, Johnson-Paben RM, Retterer ST, Yin X, Neeves KB. Single- and two-phase flow in microfluidic porous media analogs based on voronoi tessellation. Lab Chip. 2011;12(2):253–61. doi: 10.1039/c1lc20838a.

[3] Wu F, Fan QC, Huang D, Ma L, Liang XY, Sima L. Predicting gas–water relative permeability using nuclear magnetic resonance and mercury injection capillary pressure measurements. J Nat Gas Sci Eng. 2016;32:35–47. doi: 10.1016/j.jngse.2016.04.033.

[4] Wu J, Li SC, Xu ZH. Numerical analysis of gas-liquid two-phase flow after water inrush from the working face during tunnel excavation in a karst region, B. Eng Geol Environ. 2019;78(4):2973–3010. doi: 10.1007/s10064-018-1312-8.

[5] Olesen AC, Romer C, Kaer SK. A numerical study of the gas-liquid, two-phase flow maldistribution in the anode of a high pressure PEM water electrolysis cell. Int J Hydrogen Energy. 2016;41(1):52–68. doi: 10.1016/j.ijhydene.2015.09.140.

[6] Wang GC. Microscopic investigation of CO_2, flooding process. J Petrol Technol. 1982;34(8):1789–97. doi: 10.2118/9788-PA.

[7] Li J, Jiang H, Wang C, Zhao Y, Gao Y, Pei Y, et al. Pore-scale investigation of microscopic remaining oil variation characteristics in water-wet sandstone using CT scanning. J Nat Gas Sci Eng. 2017;48:36–45. doi: 10.1016/j.jngse.2017.04.003.

[8] An S, Yao J, Yang Y, Zhang W, Zhao J, Li A. The microscale analysis of reverse displacement based on digital core. J Nat Gas Sci Eng. 2017;48:138–44. doi: 10.1016/j.jngse.2016.12.014.

[9] Kumar M, Knackstedt MA, Senden TJ, Sheppard AP, Middleton JP. Visualizing and quantifying the residual phase distribution in core material. Petrophysics. 2010;51(5):323–32.

[10] Kun L, Qiang W, Mi W. Three-dimensional visualisation of gas-water two-phase flow based on bubble mapping method and size projection algorithm. Flow Meas Instrum. 2019;69:101590. doi: 10.1016/j.flowmeasinst.2019.101590.

[11] Keller AA, Bluent MJ, Roberts APV. Micromodel observation of the role of oil layers in three-phase flow. Transport Porous Med. 1997;26(3):277–97. doi: 10.1023/A:1006589611884.

[12] Li DW, Zhang LH, Zhou KM, Guo LP. Gas–water two-phase flow mechanism in visual microscopic pore model. J China U Petrol (Nat Sci). 2008;32(3):80–3, (in Chinese with English abstract). doi: 10.3321/j.issn:1673-5005.2008.03.017.

[13] Karadimitriou NK, Hassanizadeh SM. A review of micromodels and their use in two-phase flow studies. Vadose Zone J. 2012;11(3):1539–663. doi: 10.2136/vzj2011.0072.
[14] Afrapoli MS, Alipour S, Torsaeter O. Analysis of microscopic displacement mechanisms of a MIOR process in porous media with different wettability. Transport Porous Med. 2012;93:705–19. doi: 10.1007/s11242-012-9978-z.
[15] Archibong-Eso A, Shi J, Baba, Yahaya D, Aliyu M, Raji YO, et al. High viscous oil–water two-phase flow: experiments and numerical simulations. Heat Mass Transfer. 2019;55(3):755–67. doi: 10.1007/s00231-018-2461-9.
[16] Afif M, Amaziane B. Numerical simulation of two-phase flow through heterogeneous porous media. Numer Algorithms. 2003;34(2–4):117–25. doi: 10.1023/B:NUMA.0000005357.26583.3e.
[17] Huo F, Hong Z. MRT-LBM-based numerical simulation of seepage flow through fractal fracture networks. Sci China Technol Sci. 2013;56(12):3115–22. doi: 10.1007/s11431-013-5402-3.
[18] Zhang QG, Ju Y, Gong WB, Zhang L, Sun HF. Numerical simulations of seepage flow in rough single rock fractures. Petroleum. 2015;1(3):200–5.
[19] Mutailipu M, Liu Y, Wu BH, Song YC, Wang DY, Li A. Gas–water two phase flow simulation based on pore network model for reservoir rocks. Energy Proced. 2017;142:3214–9. doi: 10.1016/j.egypro.2017.12.493.
[20] Morton EJ, Luggar RD, Key MJ, Kundu A, Tavora LMN, Gilboy WB. Development of a high speed X-ray tomography system for multiphase flow imaging. IEEE T Nucl Sci. 1999;46(3):380–4. doi: 10.1109/NSSMIC.1998.774334.
[21] Xue Q, Wang HX, Yang CY. Experimental research on two-phase flow visualization using a low-energy gamma CT system with sparse projections. Meas Sci Technol. 2013;24(7):074008. doi: 10.1088/0957-0233/24/7/074008.
[22] Nie X, Zhang C, Wang C, Nie S, Zhang J, Zhang C. Variable secondary porosity modeling of carbonate rocks based on μ-CT images. Open Geosci. 2019;11(1):617–26. doi: 10.1515/geo-2019-0049.
[23] Ramstad T, Oren PE, Bakke S. Simulation of two-phase flow in reservoir rocks using a Lattice Boltzmann method. SPE J. 2010;15(4):923–33. doi: 10.2118/124617-PA.
[24] Li RR, Yang YS, Pan JX, Pereira GG, Taylor JA, Clennell B, et al. Lattice Boltzmann modeling of permeability in porous materials with partially percolating voxels. Phys Rev E: Stat Nonlinear Soft Matter Phys. 2014;90(3):1–10. doi: 10.1103/PhysRevE.90.033301.
[25] Pu H, Ni H, Xiao C. Characteristics of water sediment two phase flows in weakly cemented fractured rock mass based on Lattice Boltzmann method. J China Coal Soc. 2017;42(1):162–8. doi: 10.13225/j.cnki.jccs.2016.5011.
[26] Bakhshian S, Hosseini SA, Shokri N. Pore-scale characteristics of multiphase flow in heterogeneous porous media using the lattice Boltzmann method. Sci Rep. 2019;9(1):3377. doi: 10.1038/s41598-019-39741-x.
[27] Shah SM, Crawshaw JP, Gray F, Yang J, Boek ES. Convex hull approach for determining rock representative elementary volume for multiple petrophysical parameters using pore-scale imaging and Lattice–Boltzmann modelling. Adv Water Resour. 2017;104:65–75. doi: 10.1016/j.advwatres.2017.03.008.
[28] Sandström C, Larsson F, Runesson K, Johansson H. A two-scale finite element formulation of stokes flow in porous media. Comput Method Appl M. 2013;261–262:96–104.
[29] Lichtenfelz L, Yoneda T. A local instability mechanism of the Navier–Stokes flow with swirl on the no-slip flat boundary. J Math Fluid Mech. 2019;21(2):1–8. doi: 10.1007/s00021-019-0424-7.
[30] Frachon T, Zahedi S. A cut finite element method for incompressible two-phase Navier–Stokes flows. J Comput Phys. 2018;384:77–98. doi: 10.1016/j.jcp.2019.01.028.
[31] Faruk A, Aleksandar S, Florian F. A distributed parallel direct simulator for pore-scale two-phase flow on digital rock images using a finite difference implementation of the phase-field method. J Petrol Sci Eng. 2018;166:806–24. doi: 10.1016/j.petrol.2017.11.022.
[32] Zaretskiy Y, Geiger S, Sorbie K. Direct numerical simulation of pore-scale reactive transport: applications to wettability alteration during two-phase flow. Int J Oil Gas Coal Technol. 2012;5(2–3):142–56. doi: 10.1504/IJOGCT.2012.046318.
[33] Nick HM, Matthai SK. Comparison of three FE-FV numerical schemes for single- and two-phase flow simulation of fractured porous media. Transport Porous Med. 2011;90(2):421–44.
[34] Li H, Ranjith PG, Yamaguchi S, Sato M. Development of a 3D FEM simulator on multiphase seepage flows and its applications. Eng Appl Comp Fluid. 2007;1(3):227–37. doi: 10.1080/19942060.2007.11015195.
[35] Kolditz O, De Jonge J. Non-isothermal two-phase flow in low-permeable porous media. Comput Mech. 2004;33(5):345–64. doi: 10.1007/s00466-003-0537-x.
[36] Aziz R, Joekar-Niasar V, Martinez-Ferrer P. Pore-scale insights into transport and mixing in steady-state two-phase flow in porous media. Int J Multiphas Flow. 2018;109:51–62. doi: 10.1016/j.ijmultiphaseflow.2018.07.006.
[37] He D, Jin Y, Xue Q, Liu X, Lu S. Effect of the wettability on two-phase flow inside porous medium at nanoscale: Lattice Boltzmann simulations. J Nanosci Nanotechnol. 2017;17(9):6620–5. doi: 10.1166/jnn.2017.14423.
[38] Wu F, Wen Z, Yao C, Wang XH, Xi YP, Cong LL. Numerical simulation of the influence of pore structure on resistivity, formation factor and cementation index in tight sandstone. Acta Geol Sin. 2020;94:290–304. doi: 10.1111/1755-6724.14306.